Biochemistry

 Volume 32, Number 16 April 27, 1993

Accelerated Publications

Solution Conformation of the (+)-*cis*-*anti*-[BP]dG Adduct in a DNA Duplex: Intercalation of the Covalently Attached Benzo[*a*]pyrenyl Ring into the Helix and Displacement of the Modified Deoxyguanosine†

Monique Cosman,‡,§ Carlos de los Santos,‡,§ Radovan Fiala,‡,§ Brian E. Hingerty,‖ Victor Ibanez,⊥ Ernestina Luna,# Ronald Harvey,# Nicholas E. Geacintov,⊥ Suse Broyde,° and Dinshaw J. Patel*,‡,§

Department of Biochemistry and Molecular Biophysics, College of Physicians and Surgeons, Columbia University, New York, New York 10032, Cellular Biochemistry and Biophysics Program, Rockefeller Research Laboratories, Memorial Sloan-Kettering Cancer Center, New York, New York 10021, Health and Safety Research Division, Oak Ridge National Laboratory, Oak Ridge, Tennessee 37831, Ben May Institute, The University of Chicago, Chicago, Illinois 60637, and Chemistry and Biology Departments, New York University, New York, New York 10003

Received December 8, 1992; Revised Manuscript Received February 26, 1993

ABSTRACT: This paper reports on the solution structure of the (+)-*cis*-*anti*-[BP]dG adduct positioned opposite dC in a DNA oligomer duplex which provides the first experimentally based solution structure of an intercalative complex of a polycyclic aromatic hydrocarbon covalently bound to the N^2 of deoxyguanosine. The combined NMR–energy minimization computation studies were undertaken on the (+)-*cis*-*anti*-[BP]dG adduct embedded in the same d(C5-[BP]G6-C7)·d(G16-C17-G18) trinucleotide segment of the complementary 11-mer duplex studied previously with the stereoisomeric trans adducts. The exchangeable and nonexchangeable protons of the benzo[*a*]pyrenyl moiety and the nucleic acid were assigned following analysis of two-dimensional NMR data sets in H_2O and D_2O solution. The solution structure of the (+)-*cis*-*anti*-[BP]dG·dC 11-mer duplex has been determined by incorporating intramolecular and intermolecular proton–proton distances defined by upper and lower bounds deduced from NOESY data sets as restraints in energy minimization computations. The benzo[*a*]pyrene ring of [BP]dG6 is intercalated between intact Watson–Crick dC5·dG18 and dC7·dG16 base pairs in a right-handed DNA helix. The benzylic ring is in the minor groove while the pyrenyl ring stacks with flanking dC5 and dC7 bases on the same strand. The deoxyguanosine ring of [BP]dG6 is not Watson–Crick base paired but displaced into the minor groove with its plane parallel to the helix axis and stacks over the sugar ring of dC5. The dC17 base on the partner strand is displaced from the center of the helix toward the major groove by the intercalated benzo[*a*]pyrene ring. This intercalative structure of the (+)-*cis*-*anti*-[BP]dG·dC 11-mer duplex exhibits several unusually shifted proton resonances which can be readily accounted for by the ring current contributions of the deoxyguanosine and pyrenyl rings of the [BP]dG6 adduct. Several phosphorus resonances are shifted to low and high field of the unperturbed phosphorus spectral region and have been assigned to internucleotide phosphates centered about the [BP]dG6 modification site. These studies define the changes in the helix at the central trinucleotide segment needed to generate the intercalation site for the covalently bound (+)-*cis*-*anti*-[BP]dG adduct. Our structural studies to date permit the classification of [BP]dG adducts positioned opposite dC in DNA helices as either site II solvent-exposed structures with intact [BP]dG·dC Watson–Crick pairing as observed for the (+)-*trans*-*anti*-[BP]dG adduct [Cosman et al. (1992) *Proc. Natl. Acad. Sci. U.S.A. 89*, 1914–1918] and (–)-*trans*-*anti*-[BP]dG adduct [De los Santos et al. (1992) *Biochemistry 31*, 5245–5252] or site I intercalative structures in which the deoxyguanosine ring of [BP]dG and dC are displaced into opposite grooves and the benzo[*a*]pyrene ring intercalates into the helix as observed for the (+)-*cis*-*anti*-[BP]dG adduct in this study.

Benzo[*a*]pyrene is a ubiquitous environmental pollutant which is metabolized in living cells to highly active diol epoxide derivatives (Conney, 1982; Singer & Grunberger, 1983). Of the four biologically important bay region benzo[*a*]pyrenediol epoxide (BPDE) stereoisomers, the (+)-*anti*-7β,8α-dihydroxy-9α,10α-epoxy-7,8,9,10-tetrahydrobenzo[*a*]pyrene [(+)-*anti*-

† This research was supported by NIH Grants CA-46533 and CA-21111 to D.J.P., by NIH Training Grant CA-09503 to M.C., by NIH Grant CA-20851 and DOE Grant DE-FG02-88ER60405 to N.E.G., by NIH Grant CA-28038, NIH Grant RR-06458, and DOE Grant DE-FG02-90ER60931 to S.B., by DOE Contract DE-AC05-840R21400 with Martin-Marietta Energy Systems to B.E.H., and by NIH Grant ES-04732 and American Cancer Society Grant CN-22 to R.H.

‡ Columbia University.
§ Memorial Sloan-Kettering Cancer Center.
‖ Oak Ridge National Laboratory.
⊥ Chemistry Department, New York University.
The University of Chicago.
° Biology Department, New York University.

0006-2960/93/0432-4145$04.00/0

BPDE] enantiomer is highly tumorigenic (Buening et al., 1978; Slaga et al., 1979) and mutagenic in mammalian cells (Wood et al., 1977; Brookes & Osborne, 1982; Stevens et al., 1985). It has been implicated in the transformation of proto-oncogenes to oncogenes (Marshall et al., 1984; Barbacid, 1986; Weinberg, 1989) and is known to be toxic to replicating cells as well (Wood et al., 1977; Brookes & Osborne, 1982; Stevens et al., 1985).

When reacted with native DNA, (+)-*anti*-BPDE binds predominately to the exocyclic amino group of deoxyguanosine (N^2-dG) by trans addition to the C^{10} position (Jeffrey et al., 1976; Koreeda et al., 1976; Meehan et al., 1982), with smaller fractions undergoing cis addition at N^2-dG, as well as trans and cis addition at the exocyclic amino group of deoxyadenosine (N^6-dA) (Meehan & Straub, 1979; Cheng et al., 1989). The trans and cis nomenclature used in this paper refers to the orientation of the N^2–C^{10} covalent linkage relative to the C^9–OH bond on the benzylic ring of the BP–N^2-dG adduct. It is important to remember that the relative tumorigenic and mutagenic potentials of all of the stereospecifically defined BPDE adducts have not been explicitly established to date, with the exception of the recent site-directed mutagenesis (Basu & Essigman, 1988) study by Mackay et al. (1992), who showed that (+)-*trans-anti*-[BP]dG lesions in plasmids transformed in *Escherichia coli* lead predominantly to dG to dT transversions. While the major product by far is the (+)-*trans-anti*-[BP]dG adduct, the possible tumorigenic potential of the minor (+)-*cis-anti*-[BP]dG adduct may also be of critical importance in the expression of the biological activity of (+)-*anti*-BPDE.

It has been recognized for some time that BPDE and other metabolites with pyrene-like aromatic residues can form two types of binding sites: a site I conformation, whose spectroscopic characteristics are similar to those of classical noncovalent intercalative structures, and site II solvent-exposed conformations (Geacintov et al., 1982; Zinger et al., 1987; Harvey & Geacintov, 1988; Graslund & Jernstrom, 1989; Jankowiak et al., 1990). It has been inferred, on the basis of UV–absorbance, circular dichroism, and fluorescence spectroscopic studies of stereochemically specific (+)- and (–)-*anti*-[BP]dG adducts at the oligonucleotide level, that the trans-modified duplexes are characterized by site II solvent-exposed conformations while the cis-modified duplexes are characterized by site I intercalative-type structures (Geacintov et al., 1990, 1991; Cosman, 1991). Recently, two-dimensional NMR studies combined with energy minimization computations of the (+)-*trans-anti*-[BP]dG and (–)-*trans-anti*-[BP]-dG adducts embedded in the d(C-[BP]G-C)·d(G-C-G) sequence context at the DNA duplex level have conclusively shown that the pyrenyl residues are positioned in a widened minor groove of a minimally perturbed B-DNA helix with one face of the BP moiety forming van der Waals contacts with the sugar residues of the unmodified complementary strand, while the other face is exposed to solvent (Cosman et al., 1992; De los Santos et al., 1992). The pyrenyl ring is oriented toward the 5′-end of the modified strand in the (+)-*trans-anti*-[BP]dG adduct (Cosman et al., 1992), while it is oriented toward the 3′-end of the modified strand in the (–)-*trans-anti*-[BP]dG adduct (De los Santos et al., 1992) positioned opposite deoxycytidine at the duplex level. This remarkable orientational distinction between the two minor groove adducts, which was anticipated from energy minimization computations (Singh et al., 1991), could result in profound differences in cellular processing of these lesions (Stevens et al., 1985) and may account for the observed dissimilarities in the biological activities of the parent (+)- and (–)-*anti*-BPDE precursors.

Chart I

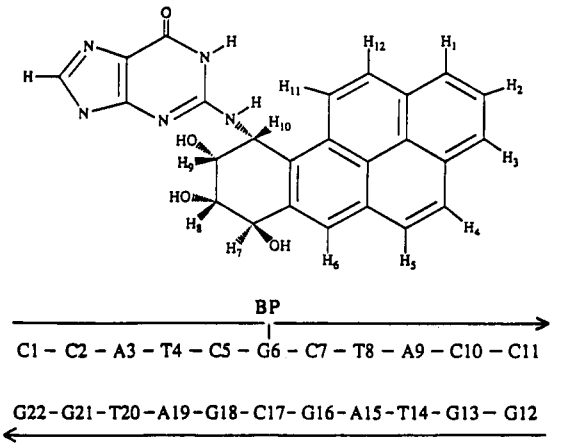

In the present paper, two-dimensional NMR studies combined with energy minimization computations are used to elucidate the solution conformation of the (+)-*cis-anti*-[BP]dG adduct **1** positioned opposite dC and flanked by dG·dC base pairs (see Chart I). The d(C-[BP]G-C)·d(G-C-G) sequence context centered at the lesion site in the 11-mer duplex **2** is the same as in earlier studies of the (+)-*trans-anti*-[BP]dG and (–)-*trans-anti*-[BP]dG adducts (Cosman et al., 1992; De los Santos et al., 1992). Our results establish that the (+)-*cis-anti*-[BP]dG adduct is characterized by intercalation of the covalently attached BP ring into the DNA helix with displacement of the modified deoxyguanosine and provide the first definitive experimental demonstration for the existence of intercalative covalent polycyclic aromatic hydrocarbon diol epoxide adducts at the DNA duplex level.

MATERIALS AND METHODS

Preparation of the (+)-cis-anti-[BP]dG·dC 11-mer Duplex. Racemic BPDE was purchased from the National Cancer Institute Chemical Carcinogen Reference Standard Repository or was synthesized in one of our laboratories (R. G. Harvey, University of Chicago). The synthesis of the (+)-*cis-anti*-BP–N^2-dG6 covalent adducts in the d(C-C-A-T-C-[BP]G6-C-T-A-C-C) sequence was carried out using previously described methods (Cosman et al., 1990) starting, however, with racemic *anti*-BPDE. Furthermore, 0.1 M triethylamine acetate (pH 6.8) was used as the reaction buffer instead of the 20 mM sodium phosphate and 0.1 M NaCl buffer, pH 7.0, previously employed, in order to increase the yield of the cis adduct (M. Cosman, L. A. Margulis, V. Ibanez, and N. E. Geacintov, unpublished). The (+)-*trans*-, (–)-*trans*-, (+)-*cis*-, and (–)-*cis-anti*-[BP]dG6 isomeric covalent adducts at the 11-mer strand level were separable by preparative HPLC on a C18 ODS Hypersil column (Cosman et al., 1990). The (+)-*cis-anti*-[BP]dG6-modified oligomer sequence was degraded with snake venom phosphodiesterase and bacterial alkaline phosphatase to characterize and verify the base composition of the modified oligomer as previously described (Cosman et al., 1990; Cosman, 1991). The modified enantiomerically pure d(C-C-A-T-C-[BP]G6-C-T-A-C-C) strand was annealed to its complementary unmodified d(G-G-T-A-G-C-G-A-T-G-G) strand at 70 °C, and the stoichiometry was followed by monitoring single proton resonances in both strands.

NMR Experiments. A combination of through-space nuclear Overhauser and through-bond correlated two-dimen-

sional spectra was recorded and analyzed to assign the carcinogen and nucleic acid protons in the (+)-*cis-anti*-[BP]-dG·dC 11-mer duplex. NOESY data sets on the modified duplex (7 mg) in H_2O buffer (0.5 mL of 0.1 M NaCl, 10 mM phosphate, 0.1 mM EDTA, pH 7.0) at 5 and 1 °C were recorded at mixing times of 100, 150, and 200 ms using a jump and return pulse for solvent suppression. The corresponding NOESY spectra in D_2O buffer at 10 °C were recorded at mixing times of 50, 200, and 300 ms. Through-bond relay connectivities in HOHAHA data sets were recorded at spin lock times of 50 and 80 ms in D_2O buffer at 10 °C.

Several factors went into the translation of the NOE intensities into the distance bounds used for the structure determination. The volume integrals of the NOE cross-peaks were measured for 200- and 300-ms mixing time NOESY data sets in D_2O and the corresponding distances calculated on the basis of the isolated two-spin approximation and the fixed deoxycytidine H6–H5 distance of 2.45 Å as a reference. The choice of upper and lower bound ranges on the estimated distances depended on the resolution of the cross-peaks in the contour plots. The base proton to sugar H1′ proton NOE cross-peaks in the 50-ms mixing time NOESY data set in D_2O were evaluated to qualitatively differentiate between syn (strong NOE) and anti (weak NOE) glycosidic torsion angles.

The coupling constant patterns for the BP(H7)-BP(H8) and BP(H9)-BP(H10) pairs were computed using the SPHINX and LINSHA programs (K. Wuthrich, ETH, Zurich) for defined puckers of the benzylic ring of [BP]dG6 in the (+)-*cis-anti*-[BP]dG·dC 11-mer duplex. These calculated coupling constant patterns, based on a modified Karplus relationship, were then compared with the experimental patterns in phase-sensitive COSY data sets.

The proton–proton vicinal coupling constants among sugar protons were analyzed from phase-sensitive COSY and DQF-COSY spectra and used to qualitatively distinguish between the different families of sugar puckers in the (+)-*cis-anti*-[BP]dG·dC 11-mer duplex. The relative intensities of the NOE cross-peaks between base protons and their own and 5′-flanking sugar H2′, H2″, and H3′ protons were also used to qualitatively distinguish between the A and B family of helices for the modified duplex (van der Ven & Hilbers, 1988).

Energy Minimization Computations. Minimized potential energy calculations were carried out with DUPLEX, a molecular mechanics program for nucleic acids that performs potential energy minimizations in the reduced variable domain of torsion angle space (Hingerty et al., 1989). The advantage of torsion space, compared to Cartesian space minimizations, is the vast diminution in the number of variables that must be simultaneously optimized, thereby permitting larger movements from a given starting conformation during minimization, as well as assurance of realistic internal geometry.

DUPLEX uses a potential set similar to one developed by Olson and co-workers for nucleic acids (Taylor & Olson, 1983), and details have been published previously (Hingerty et al., 1989). Force field parameters employed for the benzo[*a*]-pyrenediol epoxide adducts have been given previously (Hingerty & Broyde, 1985; Singh et al., 1991). In the present work the pucker of the benzylic ring of BPDE was allowed to change conformation, with all bond lengths, bond angles, and dihedral angles permitted to vary. Parameters to permit this flexibility were assigned from the AMBER force field (Weiner et al., 1986).

Å hydrogen bond penalty function (Hingerty et al., 1989) was employed in all first-stage minimizations to aid the minimizer in locating any type of designated hydrogen-bonded

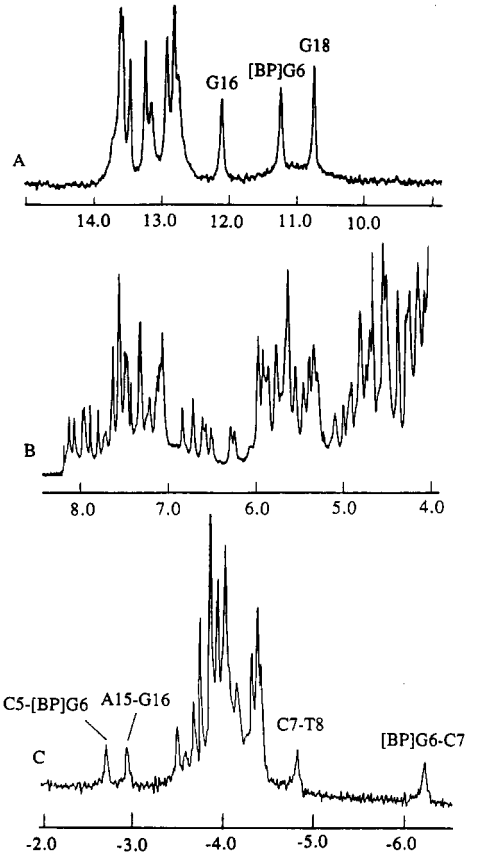

FIGURE 1: (A) The imino proton spectrum (9.0–15.0 ppm) in H_2O buffer at 5 °C, (B) the nonexchangeable proton spectrum (4.0–8.5 ppm) in D_2O buffer at 10 °C, and (C) the proton-decoupled phosphorus spectrum (–2.0 to –6.5 ppm) in D_2O buffer at 10 °C of the (+)-*cis-anti*-[BP]dG·dC 11-mer duplex. The buffer was 0.1 M NaCl, 10 mM phosphate, and aqueous solution, pH 7.0. Selevtive imino proton assignments are recorded over the spectrum in (A) and selective phosphorus assignments are recorded over the spectrum in (C).

structure or a denatured site if the function is not implemented at a particular base pair.

To locate minimum energy conformations suggested from experimental NMR data, pseudopotentials (permitting upper and lower bound restraints) were added to the energy, as described previously (Norman et al., 1989; Schlick et al., 1990). Briefly, the following functions were used:

$$F_N = W_N \sum (d - d_N)^2 \quad (1)$$

$$F_{NN} = W_{NN} \sum (d - d_{NN})^2 \quad (2)$$

The W's were adjustable weights [in the range of 10–30 kcal/(mol·Å^2)], d is the current value of the interproton distance, d_N is a target upper bound, and d_{NN} is a target lower bound. Equation 1 is implemented when d is greater than d_N, and eq 2 is implemented when d is less than d_{NN}. All penalty functions were released in the last minimization steps to yield unrestrained final structures that are energy minima.

RESULTS

Exchangeable Proton Spectra. The exchangeable proton NMR spectrum (10.0–14.0 ppm) of the (+)-*cis-anti*-[BP]dG·dC 11-mer duplex **2** in H_2O buffer, pH 7.0 at 5 °C, is plotted in Figure 1A. Three well-resolved upfield-shifted imino protons (10.8, 11.2, and 12.1 ppm) are detected in addition to the partially resolved imino protons resonating between 12.5 and 14.0 ppm. In addition, a few broader low-

intensity resonances are also present, which imply the presence of a minor conformation.

Expanded regions of the NOESY contour plot (150-ms mixing time) of the (+)-*cis-anti*-[BP]dG·dC 11-mer duplex in H_2O buffer, pH 7.0 at 5 °C, are plotted in Figure 2. The imino and amino protons in the duplex have been assigned by standard procedures [reviewed in Patel et al. (1987) and van de Ven and Hilbers (1988)]. The observed NOE patterns establish Watson–Crick pairing at all dG·dC pairs (deoxyguanosine imino to deoxycytidine amino NOE connectivities) and all dA·dT pairs (thymine imino to deoxyadenosine H2 NOE connectivities) except for the alignment of [BP]dG6 and dC17 at the modification site in the (+)-*cis-anti*-[BP]dG·dC 11-mer duplex (Figure 2B). We detect imino to imino proton NOE connectivities between all adjacent base pairs on either side of the lesion site in the duplex (peaks A–F, Figure 2A).

The imino proton of [BP]dG6 exchanges rapidly with solvent H_2O, exhibits a somewhat broadened resonance (at elevated temperatures) which is upfield shifted to 11.2 ppm (a typical value for non-hydrogen-bonded deoxyguanosine imino protons), and does not exhibit NOEs to the amino protons of dC17 positioned opposite to it on the partner strand in the duplex. Further, we do not detect an NOE between the imino proton of [BP]dG6 and the imino proton of adjacent dG16, and only a weak NOE is observed to the imino proton of adjacent dG18 (peak G, Figure 2A) centered about the lesion site. A weak intermolecular NOE between the imino proton of [BP]dG6 and the sugar H1′ proton of dC5 (peak 3, Figure 2B) suggests that the modified deoxyguanosine is positioned in the minor groove and is directed toward the 5′-end of the modified strand.

The [BP]dG6 amino proton at the covalent linkage site was difficult to assign until we realized that this amino proton overlaps with the BP(H10) proton at 6.5 ppm. Thus, a strong cross-peak is detected between the imino (11.2 ppm) and amino (6.5 ppm) protons of [BP]dG6 (peak I, Figure 2B) in the duplex. Additional evidence that the exchangeable amino proton of [BP]dG6 and the nonexchangeable BP(H10) proton are superpositioned at 6.5 ppm is as follows: (1) The intensity of the resonance at 6.5 ppm in the one-dimensional proton spectrum in H_2O solution at 5 °C decreases by approximately one-half when the water signal is saturated. (2) An exchange cross-peak is detected between the 6.5 ppm resonance and solvent H_2O in the NOESY plot of the duplex.

The imino proton of dG18 flanking the lesion site is dramatically upfield shifted to 10.8 ppm. This narrow imino proton of dG18 exhibits NOE cross-peaks to the amino protons of dC5 (peaks, J,J′, Figure 2B), both of which in turn are shifted to high field (6.9 and 5.9 ppm for the hydrogen-bonded and exposed amino protons, respectively). These results establish formation of a stable dC5·dG18 Watson–Crick base pair, and the observed large upfield shifts for the dG18 imino and dC5 amino protons may reflect stacking contributions from a large aromatic ring system such as the pyrene ring of the modified [BP]dG6 in the duplex.

The imino proton of dG16 flanking the lesion site is somewhat broader (at elevated temperatures) and exhibits a smaller upfield shift (12.1 ppm). The imino proton of dG16 exhibits NOE cross-peaks to the amino protons of dC7 (peaks H,H′, Figure 2B), both of which are also shifted to high field (7.1 and 5.9 ppm for the hydrogen-bonded and exposed amino protons, respectively). These results establish formation of a dC7·dG16 Watson–Crick base pair with the upfield shifts of the amino proton of dC7 and, to a lesser extent, the imino

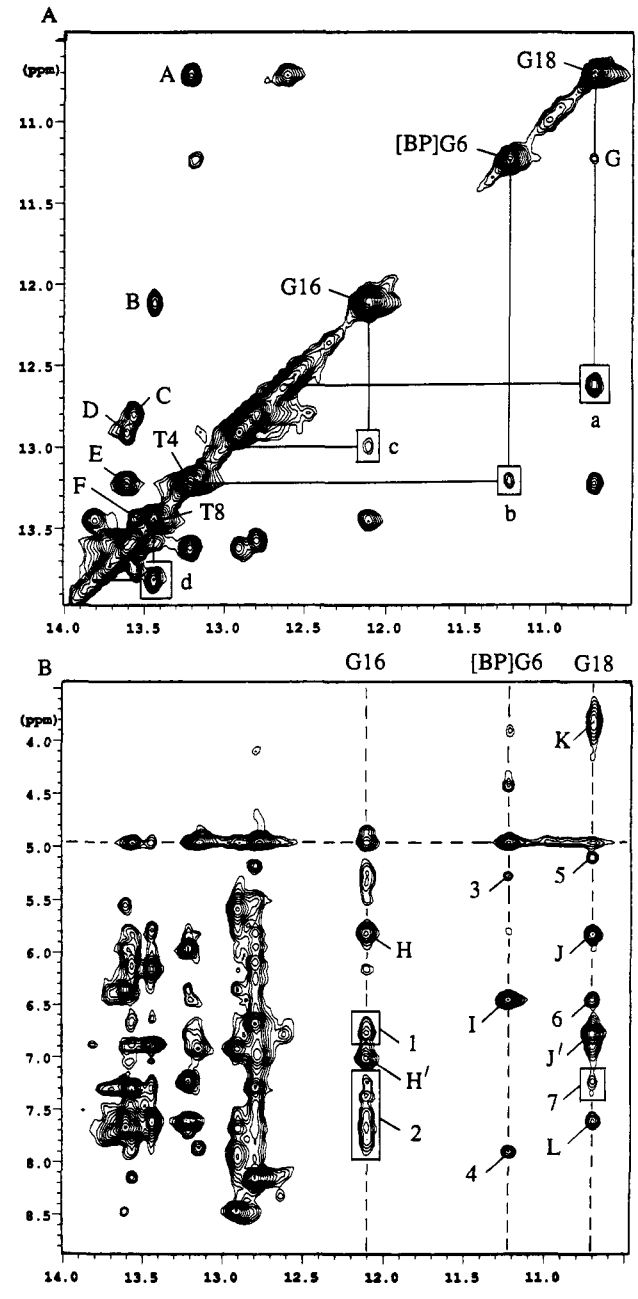

FIGURE 2: Expanded NOESY (150-ms mixing time) contour plots of the (+)-*cis-anti*-[BP]dG·dC 11-mer duplex in H_2O buffer at 1 °C. (A) NOE connectivities in the symmetrical 10.5–14.0 ppm imino proton region. The diagonal cross-peaks for the imino protons of dT4, dT8, [BP]dG6, dG16, and dG18 for the central d(T4-C5-[BP]G6-C7-T8)·d(A15-G16-C17-G18-A19) are labeled. The imino to imino NOE cross-peaks A–G are assigned as follows: A, dT4(NH3)-dG18(NH1); B, dT8(NH3)-dG16(NH1); C, dG-13(NH1)-dT14(NH3); D, dT20(NH3)-dG21(NH1); E, dT4-(NH3)-dT20(NH3); F, dT8(NH3)-dT14(NH3); G, [BP]dG6(NH1)-dG18(NH1). We detect exchange cross-peaks a–d between specific imino protons in the major and minor conformations. They are assigned as follows: a, dG18(NH1); b, [BP]dG6(NH1); c, dG16(NH1); d, dT8(NH1). (B) NOE connectivities between the imino protons (10.5–14.0 ppm) and the base and amino protons (3.5–9.0 ppm). The NOE cross-peaks involving the imino protons of dG16, [BP]dG6, and dG18 are labeled in the figure. Cross-peaks H–L are assigned as follows: H,H′, dG16(NH1)-dC7(NH_2-4h,e); I, [BP]dG6(NH1)-[BP]dG6(NH2); J,J′; dG18(NH1)-dC5(NH_2-4h,e); K, dG18(NH1)-dG18(NH_2-2) (tentative assignment); L, dG18(NH1)-dA19(H2). Cross-peaks 1–7 are assigned as follows: 1, dG16(NH1)-BP(H4,H5); 2, dG16(NH1)-BP(H1,H2,H3); 3, [BP]dG6(NH1)-C5(H1′); 4, [BP]dG6(NH1)-BP(H11); 5, dG-18(NH1)-dC5(H5)/BP(H7); 6, dG18(NH1)-BP(H10)/[BP]-dG6(NH2); 7, dG18(NH1)-BP(H3,H6).

proton of dG16, possibly reflecting stacking with the pyrene ring of [BP]dG6 in the duplex.

The observed NOE and chemical shift patterns for the central d(C5-[BP]G6-C7)·(G16-C17-G18) segment are consistent with a novel conformational alignment of [BP]dG6 and dC17 at the lesion site in the (+)-*cis-anti*-[BP]dG·dC 11-mer duplex. The covalently bound BP moiety disrupts the potential [BP]dG6·dC17 pairing alignment by positioning both the dG6 and dC17 bases outside the helix. The modified deoxyguanosine is positioned in the minor groove while the BP ring intercalates between the Watson–Crick dC5·dG18 and dC7·dG16 base pairs in the duplex.

We observe exchange cross-peaks involving the imino protons of the central d(T4-C5-[BP]G6-C7-T8)·d(A15-G16-C17-G18-A19) segment in the NOESY spectrum of the (+)-*cis-anti*-[BP]dG·dC 11-mer duplex (boxed peaks a–d, Figure 2A). These exchange cross-peaks imply a slow conformational equilibrium between the major structure which is the focus of this paper and a minor structure.

Nonexchangeable Nucleic Acid Proton Spectra. The proton NMR spectrum (4.0–8.5 ppm) of the (+)-*cis-anti*-[BP]dG·dC 11-mer duplex in D_2O buffer at 10 °C is plotted in Figure 1B. Spectral data were accumulated at low temperature due to loss of spectral resolution on raising the temperature to ambient values. Nonexchangeable proton assignments were based on an analysis of through-space distance connectivities in NOESY data sets as a function of mixing time and through-bond connectivities in COSY, DQF-COSY, and HOHAHA data sets in D_2O buffer at low temperature. Expanded NOESY (300-ms mixing time) contour plots of the (+)-*cis-anti*-[BP]dG·dC 11-mer duplex in D_2O buffer at 10 °C correlating the base protons (6.7–8.5 ppm) and the sugar H1′ protons (4.2–6.7 ppm) are plotted in Figure 3. The chain is traced from dA3 to dA9 on the modified strand (Figure 3A) and from dT14 to dT20 on the unmodified strand (Figure 3B) using sequential NOEs between the base (purine H8 or pyrimidine H6) protons and their own and 5′-flanking sugar H1′ protons. These base and sugar H1′ proton assignments have been confirmed by cross-checks in other regions of the NOESY plot which also have yielded a complete set of sugar H2′, H2″, and H3′ proton assignments. The proton chemical shifts for the central d(C5-[BP]G6-C7)·d(G16-C17-G18) segment are tabulated in Table S1 (see supplementary material). The only exception is the sugar H1′ of dC7, whose assignment is tentative at this time. We believe this resonance is broad, and hence NOE and coupling connectivities involving it are weak.

The NOE data in Figure 3 exhibit several weak cross-peaks reflecting conformational perturbations associated with the alignment of (+)-*cis-anti*-[BP]dG6 and dC17 at the lesion site in the 11-mer duplex. Thus, the NOE between the H8 proton of [BP]dG6 and the H1′ proton of dC5 in the dC5-[BP]dG6 step is very weak (box a, Figure 3A), as is that between the H6 proton of dC7 and the H1′ proton of [BP]dG6 in the [BP]dG6-dC7 step (box b, Figure 3A). We also note for the unmodified strand that the NOEs between the H6 proton of dC17 and the H1′ proton of dG16 in the dG16-dC17 step is weak (box d, Figure 3B) while that between the H8 proton of dG18 and the H1′ proton of dC17 in the dC17-dG18 step is very weak (box e, Figure 3B). The observed weak and very weak NOEs between base and their flanking sugar H1′ protons at specific steps in the d(C5-[BP]G6-C7)·d(G16-C17-G18) segment provide important distance restraints in defining the structural alignments at the covalent lesion site.

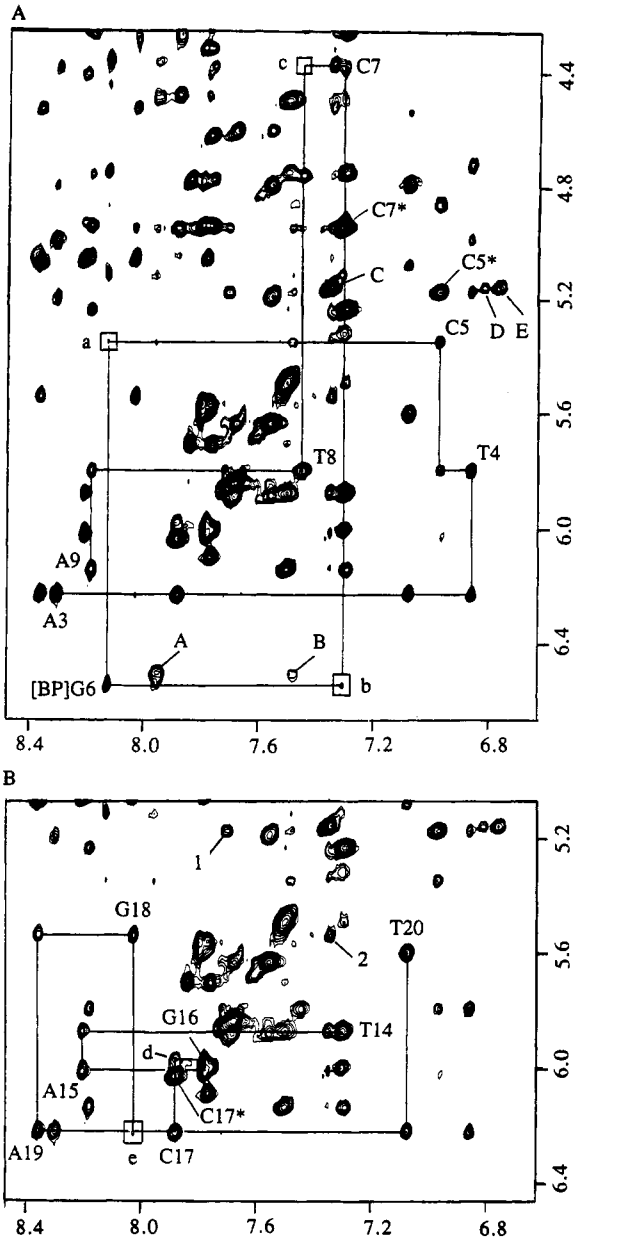

FIGURE 3: Expanded NOESY (300-ms mixing time) contour plots of the (+)-*cis-anti*-[BP]dG·dC 11-mer duplex in D_2O buffer at 10 °C establishing distance connectivities between the base (purine H8 and pyrimidine H6) protons (6.5–8.4 ppm) and the sugar H1′ and deoxycytidine H5 protons (4.2–6.7 ppm). (A) NOE connectivities between the base and their own and 5′-flanking sugar H1′ protons from dA3 to dA9 on the modified strand. The dC7(H1′) proton assignment is tentative. Cross-peaks a–c represent very weak or absent NOEs and have the following assignments: a, [BP]dG6(H8)-dC5(H1′); b, dC7(H6)-[BP]dG6(H1′); c, dT8(H6)-dC7(H1′). Cross-peaks A–E represent NOEs between BP protons and are assigned as follows: A, BP(H10)-BP(H11); B, BP(H10)-BP(H12); C, BP(H6)-BP(H7); D, BP(H4)-BP(H7); E, BP(H5)-BP(H7). The NOEs between the H5 and H6 protons of deoxycytidine are represented by C5* and C7*. (B) NOE connectivities between the base and their own and 5′-flanking sugr H1′ protons from dT14 to dT20 on the unmodified strand. Cross-peaks d and e represent weak to very weak NOEs and have the following assignments: d, dC17(H6)-dG16(H1′); e, dG18(H8)-dC17(H1′). Note the downfield shift of both the H6 and H5 protons of dC17 represented by the C17* cross-peak. The intermolecular NOE cross-peaks 1 and 2 are assigned as follows: 1, BP(H1)-dC5(H5); 2, BP(H6)-dG18(H1′). The BP benzylic and pyrenyl proton assignments in the (+)-*cis-anti*-[BP]dG·dC 11-mer duplex are as follows: BP(H1), 7.69 ppm; BP(H2), 7.37 ppm; BP(H3), 7.55 ppm; BP(H4), 6.82 ppm; BP(H5), 6.76 ppm; BP(H6), 7.34 ppm; BP(H7), 5.16 ppm; BP(H8), 4.37 ppm; BP(H9), 4.49 ppm; BP(H10), 6.49 ppm; BP(H11), 7.95 ppm; BP(H12), 7.48 ppm.

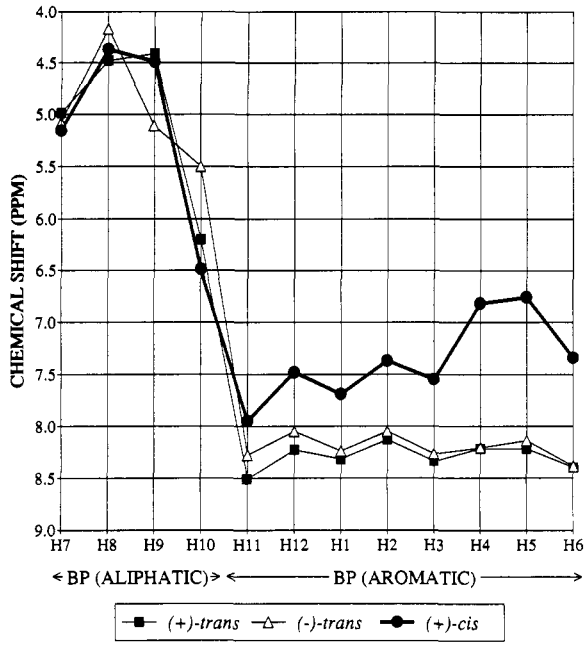

FIGURE 4: A plot comparing the benzo[*a*]pyrene ring proton chemical shifts in the (+)-*trans-anti-* (■), (−)-*trans-anti-* (△), and (+)-*cis-anti-* (●) [BP]dG6 adducts in the 11-mer duplex **2**. The benzylic protons (H7, H8, H9, H10) are on the left and the pyrenyl protons (H11, H12, H1, H2, H3, H4, H5, H6) are on the right of this plot.

We have also analyzed other regions of the NOESY contour plot of the (+)-*cis-anti*-[BP]dG·dC 11-mer duplex, and some unusual patterns observed in the data are summarized below. We observe some unusually shifted sugar H2′,2″ protons in the spectrum of the (+)-*cis-anti*-[BP]dG·dC 11-mer duplex. Thus, the H2″ proton of dC5 is shifted upfield to 1.12 ppm while the H2″ proton of [BP]dG6 is shifted downfield to 3.50 ppm (Figure S1, supplementary material). The H1′ proton of dC7 (4.4 ppm, tentative assignment) is shifted dramatically to high field though there is uncertainty as to its exact chemical shift. Such large proton shifts must reflect position-dependent ring current contributions from either the purine or pyrene aromatic ring systems.

The base H5 (6.03 ppm) and H6 (7.88 ppm) protons and the sugar H1′ (6.23 ppm) proton of dC17 are shifted to low field, strongly suggestive of displacement of this deoxycytidine from the helix axis and loss of stacking interactions. Several other nucleic acid protons exhibit less pronounced shifts in the spectrum of the (+)-*cis-anti*-[BP]dG·dC 11-mer duplex. Thus, the H5 proton of dC7 (4.95 ppm) is upfield shifted, as is that of dC5 (5.17 ppm) but to a lesser extent. Among the guanine sugar H1′ protons, that of dG18 (5.54 ppm) is shifted to high field and that of [BP]dG6 (6.54 ppm) is shifted to low field as compared to a normal value of 5.7 ppm.

Nonexchangeable Benzo[a]pyrene Protons. The nonexchangeable benzo[*a*]pyrene protons were assigned from an analysis of the through-bond and through-space connectivities in the (+)-*cis-anti*-[BP]dG·dC 11-mer duplex **2** and are tabulated in the caption to Figure 3. The pyrenyl (H11, H12, H1, H2, H3, H4, H5, and H6) protons are upfield shifted by 0.5–1.3 ppm in the (+)-*cis-anti*-[BP]dG6 adduct compared to their values in the corresponding (+)- and (−)-*trans-anti*-[BP]dG6 counterparts in the sequence context of duplex **2**. These shifts are plotted schematically in Figure 4 with the largest pyrenyl ring proton shifts observed at the BP(H4) and BP(H5) protons for the (+)-*cis-anti*-[BP]dG6 adduct stereoisomer at the duplex level. These results can be readily rationalized if the pyrene ring intercalates between dG·dC base pairs in the (+)-*cis-anti*-[BP]dG6 adduct (this study), while the pyrene ring is positioned in the minor groove in the (+)- and (−)-*trans-anti*-[BP]dG6 adducts (Cosman et al., 1992; De los Santos et al., 1992) of duplex **2**.

Intermolecular NOEs. A set of intermolecular NOEs between nonexchangeable BP protons and exchangeable and nonexchangeable nucleic acid protons have been identified and assigned in the (+)-*cis-anti*-[BP]dG·dC 11-mer duplex. The pyrenyl BP(H6) and benzylic BP(H7) protons that lie on one edge of the BP molecule exhibit NOEs to the minor groove sugar H1′ and H4′ protons of dG18 in the duplex [peak 2, Figure 3B, corresponds to the NOE between BP(H6) and G18(H1′)]. The pyrenyl BP(H1) and BP(H12) protons on the opposite edge of the BP molecule exhibit NOEs to the major groove base H5 and H6 protons of dC5 in the duplex [peak 1, Figure 3B, corresponds to the NOE between BP(H1) and dC5(H5)]. In addition, the exchangeable dG18 imino proton exhibits NOEs to specific benzylic and pyrenyl protons (peaks 5, 6, and 7, Figure 2B) while the dG16 imino proton exhibits NOEs to specific pyrenyl protons (peaks 1 and 2, Figure 2B) in the duplex. These intermolecular NOEs provide strong evidence for intercalation of the BP ring between the dC5·dG18 and dC7·dG16 base pairs and permit the definitive alignment of the various edges of the intercalated BP ring relative to the flanking dG·dC base pairs in the (+)-*cis-anti*-[BP]dG·dC 11-mer duplex.

Phosphorus Spectra. The proton-decoupled phosphorus spectrum of the (+)-*cis-anti*-[BP]dG·dC 11-mer duplex exhibits two downfield-shifted phosphorus resonances and two upfield-shifted phosphorus resonances which are outside the −3.5 to −4.5 ppm region (Figure 1C). These phosphorus resonances have been assigned from an analysis of an indirect detection proton–phosphorus heteronuclear correlation experiment (Figure S2, supplementary material). Each nonterminal phosphorus can be correlated with its 5′-linked H3′ proton (three-bond H–P coupling) and its 3′-linked H4′ proton (four-bond H–P coupling) in the two-dimensional plot (Figure S2, supplementary material), and the phosphorus resonances can be assigned on the basis of the known H3′ and H4′ proton assignments. The shifted phosphorus resonances are labeled in Figures 1C and S2 (supplementary material) with the most downfield phosphorus assigned to the dC5-[BP]dG6 step while the most upfield phosphorus is assigned to the [BP]dG6-dC7 step in the (+)-*cis-anti*-[BP]dG·dC 11-mer duplex.

Energy Minimization Computations. The search strategy employed in the present work began with an energy-minimized B-DNA (Arnott et al., 1976) central five base pair d(T4-C5-[BP]G6-C7-T8)·d(A15-G16-C17-G18-A19) segment of the (+)-*cis-anti*-[BP]dG·dC 11-mer duplex. The benzylic ring in the energy minimizations was flexible, although it was positioned with BP(H7) and BP(H8) pseudodiequatorial in the starting conformation for the minimizations, as observed for the nucleoside adduct (Cheng et al., 1989). The BP-DNA orientation space was then searched with 16 energy minimization trials in which α'[dG6(N^1)-dG6(C^2)-dG6(N^2)-BP(C^{10})] and β'[dG6(C^2)-dG6(N^2)-BP(C^{10})-BP(C^9)] were each started at 0°, 90°, 180°, and 270° in all combinations, and the DNA starting conformation was the energy-minimized B form.

In these trials, the DUPLEX hydrogen bond penalty function (Hingerty et al., 1989) for Watson–Crick base pairing was utilized at all base pairs except at the lestion site, since the NMR data indicated that the modified base pair was denatured, and NMR-derived upper- and lower-bound distance restraints were included. Searching orientation space

at 90° intervals of α' and β' is a robust procedure for locating all the important potential energy wells because our minimization protocol permits torsion angle variations of up to 100° in each minimization step (Hingerty et al., 1989). Consequently, energy minima in each quadrant of α' and β' are accessible, and the reduced variable domain of torsion angle space greatly enhances the likelihood of finding the important structures.

The 16 structures resulting from the conformational search, in which the α' and β' torsion angles were rotated by 90° intervals, were guided by the NMR distance constraints centered about the disrupted [BP]dG6·dC17 pair. These constraints included those that defined the orientation of the different edges of the intercalated planar pyrenyl ring system relative to the minor and major groove edges of the DNA helix and the stacking alignments between the intercalated pyrenyl ring and flanking dG·dC base pairs. The lowest energy structure with the best goodness of fit index could be distinguished from the other 15 structures as outlined below. We were able to eliminate 8 of the structures since they positioned the modified deoxyguanosine and the attached benzo[*a*]pyrene benzylic ring in the major groove which was at variance with the NOE between the [BP]dG6(NH1) proton and the minor groove dC5(H1′) proton observed experimentally. Four other structures were eliminated since the DNA was severely kinked with the benzo[*a*]pyrene ring either exposed to solvent or embedded into the helix with its plane parallel to the helix axis. The four remaining structures had the modified deoxyguanosine in the minor groove but differed distinctly from each other. The pyrenyl ring was not intercalated into the helix for two of these structures, and they could be eliminated from further consideration. The final two structures were of the intercalation type and differed primarily in the alignment of the modified deoxyguanosine in the minor groove. The lowest energy structure with the modified deoxyguanosine parallel to the helix axis had an energy of −188.5 kcal/mol, and the goodness of fit values for eqs 1 and 2 were respectively 19.6 and 1.7 with $W = 15$ kcal/(mol·Å^2). By contrast, the next best structure had an energy of −176.0 kcal/mol and goodness of fit indices of 24.6 and 3.9.

Consequently, the best pentamer was built, stepwise to the 11-mer duplex, by first adding a minimized B-form block of the first two duplex residues, minimizing the 7-mer, and then adding a residue at a time, following by minimization with restraints retained at each stage. Subsequently, the hydrogen bond penalty function and then the distance restraints were released with energy minimization at each step, yielding a final unrestrained structure. Convergence to very similar final constrained structures resulted when this structure was distorted by +45° or −45° at each of the two bonds (α' and β') at the base–carcinogen linkage and reminimized with constraints. Two views of the best fit superposition of the resulting four structures are plotted in Figure S3 (supplementary material). These views provide an estimate of the precision to which we can define the geometry of the intercalation site, the position of the modified dG6 and its opposing dC17, and the overlap geometry between the pyrenyl ring and the flanking base pairs at this stage of the computations.

Solution Structure. A view normal to the helix axis of the central d(T4-C5-[BP]G6-C7-T8)·d(A15-G16-C17-G18-A19) segment of the NMR–energy-minimized structure of the (+)-*cis-anti*-[BP]dG·dC 11-mer duplex is shown in Figure 5A. The [BP]dG6 and dC17 moieties are drawn as darkened bonds and clearly establish intercalation of the BP ring into the

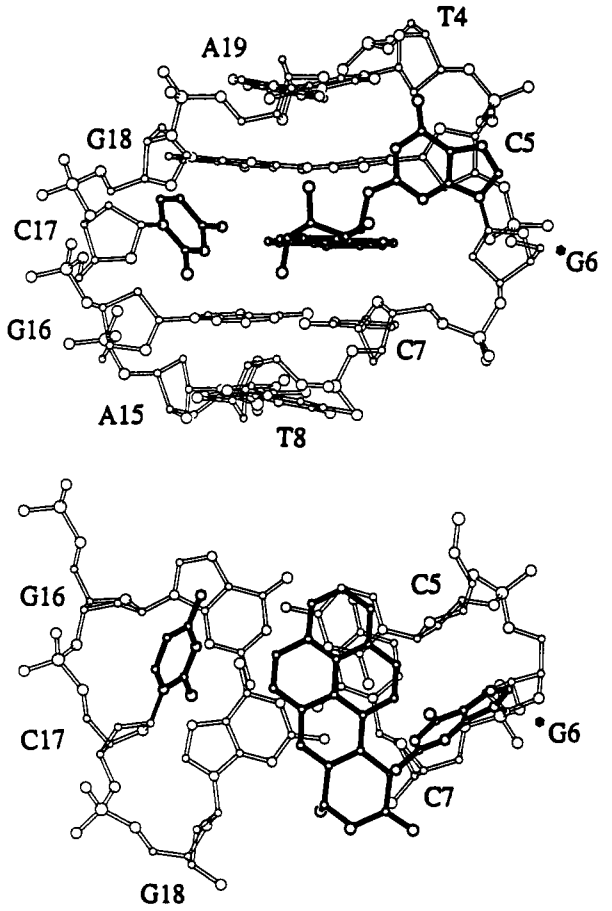

FIGURE 5: (A, top) A view looking into the minor groove and normal to the helix axis of the solution structure of the d(T4-C5-[BP]G6-C7-T8)·d(A15-G16-C17-G18-A19) segment of the (+)-*cis-anti*-[BP]dG·dC 11-mer duplex. Note that the deoxyguanosine base of [BP]dG6 is parallel to the helix axis, the benzo[*a*]pyrene ring intercalates between Watson–Crick dC5·dG18 and dC7·dG16 base pairs, and the dC17 is displaced by the intercalating chromophore. (B, bottom) A view looking down the helix axis for the central d(C5-[BP]G6-C7)·d(G16-C17-G18) segment of the solution structure of the (+)-*cis-anti*-[BP]dG·dC 11-mer duplex. Note that the benzylic ring is in the minor groove while the pyrene ring of [BP]dG6 primarily overlaps with the dC5 and dC7 bases on the same strand. Also note that dG18 overlaps to some extent with the pyrene ring in contrast to dG16. The pyrimidine base of dC17 projects toward the major groove in contrast to the purine base of [BP]dG6, which is positioned in the minor groove. The overlap geometry is such that the sugar H1′ proton of dC7 stacks over the pyrene ring, the sugar H2″ proton of [BP]dG6 is in the plane of the pyrene ring, and the sugar H2″ of dC5 stacks over the purine ring of [BP]dG6, accounting for the observed unusually large shifted chemical shift values at these protons.

helix between the dC5·dG18 and dC7·dG16 base pairs. This results in a disruption of the alignment of [BP]dG6 and dC17 such that the modified deoxyguanosine is in the minor groove pointing toward the 5′-end of the modified strand while dC17 is displaced toward the major groove. The purine base of [BP]dG6 is approximately parallel to the helix axis and stacks over the minor groove face of the dC5 sugar ring (Figure 5A).

A view down the helix axis of the central d(C5-[BP]G6-C7)·d(G16-C17-G18) segment of the NMR–energy-minimized structure of the (+)-*cis-anti*-[BP]dG·dC 11-mer duplex is shown in Figure 5B. The long axis of the BP ring is orthogonal to the long axis of the flanking dG·dC base pairs and spans both grooves of the helix. This alignment positions the nonplanar benzylic ring of BP in the minor groove while the planar pyrenyl ring of BP extends into the major groove.

The benzylic ring of BP exists as a distorted half-chair conformation with BP(H7), BP(H8), and BP(H10) in pseu-

doequatorial orientations and BP(H9) in a pseudoaxial orientation in the solution structure of the (+)-*cis-anti*-[BP]dG·dC 11-mer duplex. The experimental coupling cross-peaks BP(H7)-BP(H8) and BP(H9)-BP(H10) are well resolved in the phase-sensitive COSY spectrum, and there is good agreement between these experimental cross-peak patterns and their simulated counterparts based on three-bond vicinal proton–proton coupling constant values of ^3J(H7,H8) = 2.4 Hz, ^3J(H8,H9) = 2.7 Hz, and ^3J(H9,H10) = 5.2 Hz. The orientations of the benzylic ring substituents for the (+)-*cis-anti*-[BP]dG6 adduct in the 11-mer duplex established in the present study are in agreement with similar conclusions based on experimental studies at the nucleoside level (Cheng et al., 1989).

The carcinogen–base linkage site for the [BP]dG6 residue is defined by the angles α'[dG6(N^1)-dG6(C^2)-dG6(N^2)-BP(C^{10})] = 160° and β'[dG6(C^2)-dG6(N^2)-BP(C^{10})-BP(C^9)] = 136° in the NMR–energy-minimized structure of the (+)-*cis-trans*-[BP]dG·dC 11-mer duplex.

The glycosidic torsion angles, sugar puckers, and backbone torsion angles for the d(C5-[BP]G6-C7)·d(G16-C17-G18) segment of the NMR–energy-minimized structure of the (+)-*cis-anti*-[BP]dG·dC 11-mer duplex are given in Table S2 (supplementary material). We note that the sugar pseudorotation parameter (Altona & Sundaralingam, 1972) of C5 is P = 51° (C4′-exo pucker) in contrast to the other sugars which are centered around P = 180° (C2′-endo pucker). The glycosidic torsion angles χ = 189° for [BP]dG6 and χ = 322° (high anti value) for dC17 differ from the values for other residues which are centered around χ = 240°. The remaining backbone torsion angles in the central segment fall in or very near the normal unperturbed B_I-DNA region despite generation of the benzo[*a*]pyrene intercalation site and displacement of both dG6 and dC17 positioned opposite it.

DISCUSSION

Conformational Equilibrium. We have observed reasonably well resolved exchangeable (Figure 1A), nonexchangeable (Figure 1B), and phosphorus (Figure 1C) spectra for the (+)-*cis-anti*-[BP]dG·dC 11-mer duplex which have permitted assignment of base and sugar protons and backbone phosphates of the major conformation following analysis of homonuclear and heteronuclear two-dimensional NMR data sets. The only assignment uncertainty at the current time is the chemical shift of the sugar H1′ proton of dC7, which we believe is broad, based on the very weak NOEs to its own sugar H2′,2″ protons. Several exchangeable (Figure 1A) and nonexchangeable (Figure 1B) protons undergo large upfield shifts which primarily reflect ring current contributions from the pyrene ring of [BP]dG6.

The observation of exchange cross-peaks involving imino protons in the central d(T4-C5-[BP]G6-C7-T8)·d(A15-G16-C17-G18-A19) segment of the (+)-*cis-anti*-[BP]dG·dC 11-mer duplex (peaks a–d, Figure 2A) has established a slow equilibrium between the major conformation which is the focus of this paper and a minor conformation. We have been unable to characterize this minor conformation in any detail but put forward qualitative conclusions regarding structural features based on the range of its imino proton chemical shifts. The imino protons of [BP]dG6 (13.21 ppm), dG16(13.01 ppm), and dG18(12.63 ppm) are characteristic of deoxyguanosine imino protons of dG·dC base pairs in regular duplexes. These results suggest formation of the [BP]dG6·dC17 base pair, and the absence of a large upfield shift at the dG16 and dG18 imino protons suggests that the pyrene ring does not intercalate into the helix in the minor conformation of the (+)-*cis-anti*-[BP]dG·dC 11-mer duplex in solution.

NOE and Chemical Shift Patterns. The solution structure of the major conformation of the (+)-*cis-anti*-[BP]dG·dC 11-mer duplex shown in Figure 5 establishes that the covalently attached benzo[*a*]pyrene ring intercalates between intact Watson–Crick dC5·dG18 and dC7·dG16 base pairs and displaces dC17 positioned opposite it on the partner strand. Further, the deoxyguanosine ring of [BP]dG6 is positioned in the minor groove and parallel to the helix axis. This unusual structural alignment for [BP]dG6 should result in novel NOE and chemical shift patterns distinct from unperturbed helices. This structure must not only satisfy the distance restraints but also be consistent with the observed chemical shift changes associated with intercalation of the pyrene ring into the helix.

Let us start by evaluating whether the intermolecular NOE-based distance restraints between benzo[*a*]pyrene and flanking dG·dC base pairs are satisfied by the structure (Table S3, supplementary material). The BP ring edge containing the BP(H6) and BP(H7) protons is directed toward the minor groove face of the dG18 sugar in the structure (Figure 5B), which accounts for the NOEs between the sugar H1′ proton of dG18 and the H6 and H7 protons of BP observed experimentally. The BP ring edge containing the BP(H1) and BP(H2) protons is stacked over the base protons of dC5 in the structure (Figure 5B), which accounts for the NOEs between the H6 and H5 protons of dC5 and the H1 proton of BP observed experimentally.

The very weak NOEs (200- and 300-ms mixing time NOESY data sets) observed between base protons (purine H8 and pyrimidine H6) and the 5′-flanking sugar H1′ protons for steps centered about the intercalation site (Figure 3) are consistent with the corresponding interproton distances in the structure of the (+)-*cis-anti*-[BP]dG·dC 11-mer duplex. These distances are 4.58 Å for the dC5-[BP]dG6 step, 5.41 Å for the [BP]dG6-dC7 step, and 5.74 Å for the dG16-dC17 step. The distance is short for the dC17-dG18 step in contrast to the very weak NOE between the H6 proton of dG18 and the H1′ proton of dC17 observed experimentally (Figure 3B). However, dC17 represents the least well defined portion of the structure, and the significance of the discrepancy is uncertain at this time.

Let us next evaluate whether the observed proton chemical shift changes can be explained by the overlap geometries between the bezo[*a*]pyrene ring and the flanking dG·dC base pairs in the structure. The pyrene ring protons experience upfield ring current shifts from the flanking dG·dC base pairs over which they stack in the (+)-*cis-anti*-[BP]dG·dC 11-mer duplex, and the largest shifts would be predicted and are observed experimentally for BP(H4) and BP(H5) protons (Figure 4) which are positioned closest to the helix axis (Figure 5B). Since the benzylic ring does not stack over adjacent dG·dC base pairs in the (+)-*cis-anti*-[BP]dG·dC 11-mer duplex (Figure 5B), its protons (H7, H8, H9, and H10) exhibit chemical shifts that are similar to the corresponding values observed for the (+)- and (−)-*trans-anti*-[BP]dG6 stereoisomers (Figure 4) in the sequence context of duplex **2**.

The pyrenyl ring of [BP]dG6 stacks primarily with the flanking dC5 and dC7 bases on the same strand in the structure (Figure 5B). The imino proton of dG18 is positioned more directly over the pyrenyl ring while the imino proton of dG16 projects onto the periphery of the pyrenyl ring (Figure 5B). These stacking arrangements account for the upfield shifts for the amino protons of dC5 and dC7 and the larger upfield shift for the imino proton of dG18 compared to the imino

proton of dG16 observed experimentally. The ring currents of the pyrenyl ring of [BP]dG6 also account for several unusual proton chemical shifts observed experimentally in the (+)-*cis-anti*-[BP]dG·dC 11-mer duplex. Thus, the H2″ proton of [BP]dG6 is shifted downfield since it is in the plane of the pyrene ring (Figure 5A) while the H1′ proton of dC7 is shifted upfield since it is partially stacked over the pyrene ring in the structure (Figure 5B).

Both the deoxyguanosine ring of [BP]dG6 and the deoxycytidine ring of dC17 are displaced out of the helix axis at the intercalation site in the structure of the (+)-*cis-anti*-[BP]dG·dC 11-mer duplex. The deoxyguanosine ring is positioned in the minor groove with its plane parallel to the helix axis and stacked over the minor groove edge of the sugar ring of dC5 in the structure (Figure 5A). This alignment accounts for the weak NOE between the imino proton of [BP]dG6 and the sugar H1′ proton of dC5 observed experimentally (Figure 2B). The upfield chemical shifts observed for the minor groove sugar H1′ and H2″ protons of dC5 must reflect stacking of these protons over the deoxyguanosine ring of [BP]dG6 in the structure.

The dC17 base is displaced out of the helix, positioned in the major groove, and does not stack with flanking dG·dC base pairs in the structure (Figure 5). Such an alignment readily explains the downfield-shifted position of the H6, H5, and H1′ protons of dC17 in the NOESY spectrum of the complex (Figure 3B). The precise alignment of dC17 remains uncertain since the NOEs between the base protons of dC17 and adjacent sugar protons are very weak in the experimental spectrum, and hence its position is poorly defined by the distance restraints.

Intercalation Site. A key feature of the (+)-*cis-anti*-[BP]dG·dC 11-mer is intercalation of the pyrene ring and displacement of the modified deoxyguanosine and its opposing deoxycytidine on the partner strand, thus disrupting the modified dG·dC pair (Figure 5). This intercalation site is distinct from structures of anthracyclines covalently linked through their amino sugars to the N^2 of deoxyguanosines where the aglycon intercalates one base pair removed in the 3′-direction from the covalently modified dG·dC Watson–Crick base pair (Wang et al., 1991; Gopalakrishnan & Patel, 1993). Similarly, the intercalation site is distinct from structures of the food toxins aflatoxin and sterigmatocystin covalently linked to the N^7 of deoxyguanosines where the chromophore intercalates in the 5′-direction adjacent to the covalently modified dG·dC Watson–Crick base pair (Gopalakrishnan et al., 1990, 1992).

Another unusual feature of the structure of the (+)-*cis-anti*-[BP]dG·dC 11-mer duplex is the orientation of the deoxyguanosine ring of [BP]dG6, which is parallel to the helix axis in the minor groove and directed toward the 5′-end of the modified strand (Figure 5A). To our knowledge there is only one other example of a base aligned parallel to the helix axis, and this has been reported for the *cis*-$Pt(NH_3)_2$ adduct coordinated to the N^7 atoms of nonadjacent deoxyguanosines in the d(*G-T-*G)-d(C-A-C) segment embedded in a DNA duplex [reviewed in Patel (1992)].

The glycosidic and backbone torsion angles and sugar pucker pseudorotation angles for the d(C5-[BP]G6-C7)·d(G16-C17-G18) segment of the (+)-*cis-anti*-[BP]dG·dC 11-mer duplex listed in Table S2 (supplementary material) establish that the intercalation site is generated with minimal perturbation in the torsion angles from B-DNA (Drew et al., 1981). The primary changes are at the sugar pseudorotation angle of dC5 and the glycosidic torsion angles of [BP]dG6 and dC17. Despite this conformity with essentially standard B_I-DNA conformation, the backbone phosphate of dC5-[BP]dG6 is shifted to lowest field and that of [BP]dG6-dC7 is shifted to highest field in the phosphorus spectrum of the (+)-*cis-anti*-[BP]dG·dC 11-mer duplex (Figure 1C). The downfield shift of the dC5-[BP]dG6 phosphate may reflect, in part, in-plane ring current contributions from the intercalated pyrene ring (Figure 5A). We have no explanation for the origin of the upfield shift of the [BP]dG6-dC7 phosphate at this time.

It should be noted that the long axis of the intercalated pyrene ring is orthogonal to the long axis of the flanking dG·dC base pairs in the (+)-*cis-anti*-[BP]dG·dC 11-mer duplex (Figure 5B), similar to what has been observed for alignment of the intercalated aglycon relative to the flanking base pairs in anthracycline intercalation complexes [reviewed in Wang (1992)]. The helical twist between the dC5·dG18 and the dC7·dG16 base pairs in the (+)-*cis-anti*-[BP]dG·dC 11-mer duplex is calculated to be 67° (Babcock & Olson, 1992). This is not far from the 68–70° average value expected for B-DNA in solution, with 10.3–10.6 base pairs per turn (Wang, 1979; Rhodes & Klug, 1980) and, consequently, a twist of 34–35° per base pair.

Conclusion. The conformation of adducts derived from the covalent binding of *anti*-BPDE to DNA, especially the prevalence of external or intercalative structures, has long been a subject of controversy (Geacintov et al., 1978; Hogan et al., 1981). This NMR study of the (+)-*cis-anti*-[BP]dG adduct, as well as previous NMR investigations of the analogous (+)- and (−)-*trans-anti*-[BP]dG oligonucleotide adducts (Cosman et al., 1992; De los Santos et al., 1992), shows that both types of conformations are possible. The two trans adducts [derived from the (+)- and (−)-enantiomers of *anti*-BPDE] exhibit external site II conformations with the pyrenyl residue situated in the minor groove, while in the site I-type (+)-cis adduct, the pyrenyl ring system is intercalated in an unconventional manner with the linked deoxyguanosine residue displaced into the minor groove. These findings provide unambiguous structural rationalizations for the earlier site I/site II classification of adduct types which were based solely on optical spectroscopic data (Geacintov et al., 1982). While the solution structure of the (−)-*cis-anti*-[BP]dG adduct has not yet been determined by high-resolution NMR methods, optical spectroscopic studies carried out with polynucleotides and oligonucleotides modified covalently with (+)- and (−)-*anti*-BPDE suggest that both cis adducts are characterized by site I conformations, while trans adducts exhibit site II structures (Geacintov et al., 1991; Cosman, 1991).

High-resolution NMR techniques and the availability of BPDE-modified deoxyoligonucleotides in sufficiently large quantities for detailed structural studies have provided new insights into the relationships between the stereochemical and conformational properties of N^2-dG lesions derived from the two different enantiomers of *anti*-BPDE. The detailed structural information on these and other adducts, which already have been or will be generated by these approaches, should provide an important impetus for interpreting chemical structure–biological activity relationships in enzymatic repair, site-directed mutagenesis, and eventually tumorigenesis, initiated by the reactions of this class of chemicals with DNA.

This contribution briefly outlines the main conclusions of the NMR–energy minimization studies on the (+)-*cis-anti*-[BP]dG·dC 11-mer duplex which have identified for the first

time a base-displaced intercalation-type structure for a polycyclic aromatic hydrocarbon covalently attached to N^2 of the deoxyguanosine adduct at the DNA oligomer level. A detailed account of NMR spectral assignments and distance and coupling restraints, as well as back-calculation computations using molecular dynamics algorithms, will be described elsewhere on completion of ongoing experiments.

ACKNOWLEDGMENT

Computations were performed on the Cray supercomputers at the DOE National Energy Research Supercomputer Center and the NSF San Diego supercomputer. One of us (S.B.) wishes to thank Drs. R. Shapiro and S. B. Singh for helpful discussions. We thank Marla Babcock for the calculation of twist angles.

SUPPLEMENTARY MATERIAL AVAILABLE

Three tables listing proton chemical shifts of the central trinucleotide segment (Table S1), backbone torsion angles of the lowest energy structure for the central trinucleotide segment (Table S2), and a comparison of experimental distance bounds between benzo[*a*]pyrene and DNA protons with observed values for the lowest energy structure (Table S3) and three figures showing an expanded NOESY contour plot between the base proton and sugar H2′,2″ proton regions (Figure S1), a heteronuclear ^1H–^{31}P correlation contour plot (Figure S2), and the superposition of four structures derived following energy minimization with constraints from the lowest energy structure in which the α' and β' angles were changed by ±45° (Figure S3) (6 pages). Ordering information is given on any current masthead page.

REFERENCES

Altona, C., & Sundaralingam, M. (1972) *J. Am. Chem. Soc. 94*, 8205–8212.

Arnott, S., Bond, P. J., Selsing, E., & Smith, P. J. (1976) *Nucleic Acids Res. 3*, 2459–2470.

Babcock, M. S., & Olson, W. K. (1992) A new program for the analysis of nucleic acid structure: Implications for nucleic acid structure interpretation, in *Computation of Biomolecular Structures: Achievements, Problems, Perspectives* (Soumpasis, D. M., & Jovin, T. M., Eds.) Springer-Verlag, Heidelberg (in press).

Barbacid, M. (1986) *Carcinogenesis 7*, 1037–1042.

Basu, A., & Essigman, J. M. (1988) *Chem. Res. Toxicol. 1*, 1–18.

Brookes, P., & Osborne, M. R. (1982) *Carcinogenesis 3*, 1223–1226.

Buening, M. K., Wislocki, P. G., Levin, W., Yagi, H., Thakker, D. R., Akagi, H., Koreeda, M., Jerina, D. M., & Conney, A. H. (1978) *Proc. Natl. Acad. Sci. U.S.A. 75*, 5358–5361.

Cheng, S. C., Hilton, B. D., Roman, J. M., & Dipple, A. (1989) *Chem. Res. Toxicol. 2*, 334–340.

Conney, A. H. (1982) *Cancer Res. 42*, 4875–4917.

Cosman, M. (1991) Ph.D. Dissertation, New York University, New York.

Cosman, M., Ibanez, V., Geacintov, N. E., & Harvey, R. G. (1990) *Carcinogenesis 11*, 1667–1672.

Cosman, M., De los Santos, C., Fiala, R., Hingerty, B. E., Singh, S. B., Ibanez, V., Margulis, L., Live, D., Geacintov, N. E., Broyde, S., & Patel, D. J. (1992) *Proc. Natl. Acad. Sci. U.S.A. 89*, 1914–1918.

De los Santos, C., Cosman, M., Hingerty, B. E., Ibanez, V., Margulis, L. A., Geacintov, N. E., Broyde, S., & Patel, D. J. (1992) *Biochemistry 31*, 5245–5252.

Drew, H., Wing, R., Takano, T., Broka, C., Tanaka, S., Itakura, K., & Dickerson, R. E. (1981) *Proc. Natl. Acad. Sci. U.S.A. 78*, 2179–2183.

Geacintov, N. E., Gagliano, A. G., Ivanovic, V., & Weinstein, I. B. (1978) *Biochemistry 17*, 5256–5262.

Geacintov, N. E., Giagliano, A. G., Ibanez, V., & Harvey, R. G. (1982) *Carcinogenesis 3*, 247–253.

Geacintov, N. E., Cosman, M., Ibanez, V., Birke, S. S., & Swenberg, C. E. (1990) in *Molecular Basis of Specificity in Nucleic Acid–Drug Interactions* (Pullman, B., & Jortner, J., Eds.) pp 443–450, Kluwer Academic Publishers, Dordrecht, The Netherlands.

Geacintov, N. E., Cosman, M., Mao, B., Alfano, A., Ibanez, V., & Harvey, R. G. (1991) *Carcinogenesis 12*, 2099–2108.

Gopalakrishnan, S., & Patel, D. J. (1993) *Biochemistry* (submitted for publication).

Gopalakrishnan, S., Harris, T. M., & Stone, M. P. (1990) *Biochemistry 29*, 10438–10448.

Gopalakrishnan, S., Liu, X., & Patel, D. J. (1992) *Biochemistry 31*, 10790–10801.

Graslund, A., & Jernstrom, B. (1989) *Q. Rev. Biophys. 22*, 1–37.

Harvey, R. G., & Geacintov, N. E. (1988) *Acc. Chem. Res. 21*, 66–73.

Hingerty, B. E., & Broyde, S. (1985) *Biopolymers 24*, 2279–2299.

Hingerty, B. E., Figueroa, S., Hayden, T., & Broyde, S. (1989) *Biopolymers 28*, 1195–1222.

Jankowiak, R., Lu, P.-Q., Small, G., & Geacintov, N. E. (1990) *Chem. Res. Toxicol. 3*, 39–46.

Jeffrey, A. M., Jennette, K. W., Blobstein, S. H., Weinstein, I. B., Beland, F. A., Harvey, R. G., Kasai, H., Miura, I., & Nakanishi, K. (1976) *J. Am. Chem. Soc. 98*, 5714–5715.

Koreeda, M., Moore, P. D., Yagi, H., Yeh, H. J., & Jerina, D. M. (1976) *J. Am. Chem. Soc. 98*, 6720–6722.

Mackay, W., Benasutti, M., Drouin, E., & Loechler, E. L. (1992) *Carcinogenesis 13*, 1415–1425.

Marshall, C. J., Vousden, K. H., & Phillips, D. H. (1984) *Nature 310*, 586–589.

Meehan, T., & Straub, K. (1979) *Nature 277*, 410–412.

Meehan, T., Gamper, H., & Becker, J. F. (1982) *J. Biol. Chem. 257*, 10479–10485.

Norman, D., Abuaf, P., Hingerty, B. E., Live, D., Grunberger, D., Broyde, S., & Patel, D. J. (1989) *Biochemistry 28*, 7462–7476.

Patel, D. J. (1992) *Curr. Opin. Struct. Biol. 2*, 345–353.

Patel, D. J., Shapiro, L., & Hare, D. (1987) *Q. Rev. Biophys. 20*, 35–112.

Rhodes, D., & Klug, A. (1980) *Nature 286*, 573–578.

Schlick, T., Hingerty, B. E., Peskin, C. S., Overton, M. L., & Broyde, S. (1990) in *Theoretical Chemistry and Molecular Biophysics* (Beveridge, D., & Lavery, R., Eds.) pp 39–58, Academic Press, New York.

Singer, B., & Grunberger, D. (1983) *Molecular Biology of Mutagens and Carcinogens*, Plenum Press, New York.

Singh, S. B., Hingerty, B. E., Singh, U. C., Greenberg, J. P., Geacintov, N. E., & Broyde, S. (1991) *Cancer Res. 51*, 3482–3492.

Slaga, T. J., Bracken, W. J., Gleason, G., Levin, W., Yagi, H., Jerina, D. M., & Conney, A. H. (1979) *Cancer Res. 39*, 67–71.

Stevens, C. W., Bouck, N., Burgess, J. A., & Fahl, W. E. (1985) *Mutat. Res. 152*, 5–14.

Taylor, E. R., & Olson, W. K. (1983) *Biopolymers 22*, 2667–2702.

van de Ven, F. J., & Hilbers, C. W. (1988) *Eur. J. Biochem. 178*, 1–38.
Wang, A. H. J. (1992) *Curr. Opin. Struct. Biol. 2*, 361–368.
Wang, A. H. J., Gao, Y. G., Liaw, Y. C., & Li, Y. K. (1991) *Biochemistry 30*, 3812–3815.
Wang, J. C. (1979) *Proc. Natl. Acad. Sci. U.S.A. 76*, 200–203.
Weinberg, R. A. (1989) *Cancer Res. 49*, 3713–3721.
Weiner, S., Kollman, P. A., Nguyen, D. T. J., & Case, D. A. (1986) *J. Comput. Chem. 7*, 230–252.
Wood, A. W., Chang, R. L., Levin, W., Yagi, H., Thakker, D. R., Jerina, D. M., & Conney, A. H. (1977) *Biochem. Biophys. Res. Commun. 77*, 1389–1396.
Zinger, D., Geacintov, N. E., & Harvey, R. G. (1987) *Biophys. Chem. 27*, 131–138.